

Vibration analysis of low-field MRI using finite element analysis and experimental approach

Swapnil ARAWADE¹, Janusz PIECHOWICZ¹, Tadeusz PAŁASZ²

¹ AGH University of Krakow, Al. Adama Mickiewicza 30, 30-059 Kraków, Poland

Corresponding author: Swapnil ARAWADE, email: sarawade@agh.edu.pl

Abstract Magnetic Resonance Imaging (MRI) is powerful tool to diagnose human body. The vibration of gradient coil during image acquisition can degrade image quality. In this study, the vibration characteristics of the low field open configuration MRI system is investigated through finite element (FE) analysis and experimental measurements. The FE model was subjected to the harmonic excitation with Lorentz force and moments for pairs of X, Y and Z gradient coils individually and simultaneously. The acceleration measurements were acquired for generating slice, phase encoding and readout gradient types for different scan orientations. Results revealed that FE model predicts the vibration characteristics accurately with 1.15 % average deviation. The time and frequency domain results from the experimental investigations are important in understanding dynamic behaviour of gradient coil of MRI system for designing vibration attenuation strategy in MRI systems.

Keywords: gradient coil, magnetic resonance, vibration, noise, FEA.

1. Introduction

Magnetic resonance (MR) imaging (MRI) is important non-invasive diagnostic tool in modern medicine. It has become the gold standard for image acquisition for soft tissue and bones [1-6]. The main safety advantage of MRI is that it does not expose patients to ionizing radiation. MRI systems are generally classified as closed or open configuration systems, which are further subcategorized into low field and high field systems depending upon the magnetic field strength of magnets. Generally, MR systems with magnetic field strength less than 1.5 Tesla are considered as low field MRI system. Low field MRI systems have advantage of cheap manufacturing, less power consumption and maintenance, high safety, but generates images with lower resolution as compared to high field MRI systems [7, 8]. The Low field MRI systems are sensitive to vibration and can lead to degraded signal to noise ratio (SNR) in the images which may result in blurring effects or artefacts during image acquisition [9-11].

During image acquisition, the gradient coils in the MRI system generates the linearly varying dynamic magnetic field inside the scanning zone. There are three types of magnetic gradients applied along the three orthogonal axes (viz. X, Y and Z). The slice selection gradient is applied to locate and isolate specific plane or slice for imaging in the scanning zone. Then the Radio-Frequency (RF) excitation of protons in the slice region is executed by RF coil. Phase encoding and frequency readout gradients encode each voxel in the selected slice with the phase shift and resonant frequency value of protons [12, 13]. To produce the magnetic gradient in the scanning zone, the coils are subjected to fast switching alternating current, which interacts with the static magnetic field and sets the current carrying coils in vibration developing the Lorentz forces [14]. The vibrations originated from the gradient coils propagates through structure of system and reach to scanning zone subjecting test specimen to vibration. The interaction of vibrating surface with surrounding media which is air, generates typical sound of MRI scanning [15-17]. In case of high field MRI systems, the sound pressure level (SPL) inside the scanning room may exceed 100 dB and longer exposure to such SPL can be harmful for patient [18-22].

Scientific publications in the field have presented many approaches to improve the vibration and noise associated with the MRI systems. These methods involve modification in MRI system design, modification of operating condition, isolation of generated vibration. A simulation study on design of gradient coil presented in [23] used boundary element method (BEM) to obtain coil patterns which resulted in improved vibroacoustic performance showing 3 dB quieter operation compared to conventional design. A successful modification of gradient coil to axisymmetric design presented in [24] leads to reduced vibration and noise

² Jagiellonian University in Krakow, ul. Gołębia 24, 31-007 Kraków, Poland

in the MRI system. The coil design presented in [25] by using inverse boundary element method for controlled Lorentz forces in presence of static magnetic field of MRI system. Authors mentioned applicability of presented methodology to improve the mechanical stability of the gradient coils during image acquisition. Gradient pulse modification is more feasible approach as compared to performing modification in the hardware of MRI scanner. Recently, the study [26] presented sequence optimization method to modify the characteristics of the input current to the gradient coil which resulted in 18.6 dB quieter operation of MRI system indicating lowered vibration of gradient coil. Also, near silent gradient coil operation was reported in [27] by configuring the echo time to zero in the scanning sequence. Vibration and noise isolation technique on 7 Tesla MRI scanner was implemented in [28] by modifying pathways for vibration and sound propagation.

The literature published have addressed the problem and different methods to mitigate the vibration and resultant noise from the MRI systems. However, a better solution is still needed, as drastic hardware modifications are not feasible due to well established conventional design and involvement of high costs. Also, modifications in the scanning sequences have shown to compromise the image quality [29, 30]. To develop the better vibration mitigation strategy, it is important to thoroughly understand the characteristics of the vibration source. The objective of this study was to develop a computational model to predict and experimentally validate the vibration characteristics of the gradient system in low-field open configuration MRI scanner. The study investigates the influence of gradient type and scanning orientation on dynamics of vibration. The results from the study will be useful in vibration attenuation technique in low field MRI scanners as well as developing the acoustic noise reduction strategy for high field MRI systems.

2. Materials and methods

In this study, vibration characteristics of the low magnetic field MRI scanner with static magnetic field strength (B_0) of 89 mT (Make: MRI-Tech) are analysed. In open configuration of MRI scanner, the gradient surface coils setup with 40 mT/m strength is arranged at top and bottom of the scanning zone and the radio frequency coil encloses the scanning zone. There are 3 commonly used scanning orientations on the MRI imaging namely transverse, sagittal, and coronal, where transverse refers to imaging planes perpendicular to body's long axis, coronal to planes dividing into front and back and sagittal to planes dividing into left and right.

2.1. Finite element analysis of the lower gradient coil set

A finite element analysis (FEA) was performed to study the vibration properties of the gradient coil set during operation. ANSYS Mechanical was used to develop and analyse a 3-D model of the gradient coil set. The FEA model is shown in Fig. 1 a) and arrangement of the lower gradient coil set is shown in the Fig. 1 b). Model consists of total 19 layers of static field coil, primary and shield X, Y and Z gradient coils, a layer of material which simulate water cooling tube and intermediate layers of epoxy-based laminations and adhesive material. The dimensions and the material properties of the FE model were taken from the original design specifications.

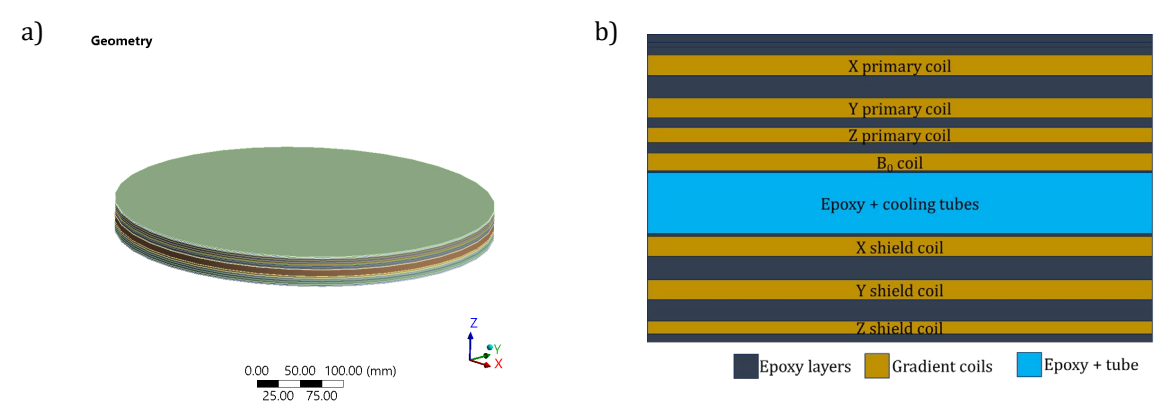


Figure 1. Finite element model of the lower gradient coil set of low field MRI device showing: a) FEA model b) arrangement of the gradient coil set.

The gradient coil set under investigation has outer diameter of 440 mm and total thickness of 37 mm. The gradient coils are conducing sheets having thickness of 1.57 mm with winding pattern etched with appropriate current density distribution sufficient to produce the required gradient field of 40 mT/m. The

Young's modulus of the copper and epoxy laminates were 110 GPa and 1.8 MPa respectively at room temperature. To avoid computational complications, the material properties were assumed to remain constant in the frequency range of interest. In the pre-processing of the model the etched grooves on the gradient coil surface were eliminated for geometry clean up and simplification. In the model there are a total of 46162 elements and 54105 nodes. The boundary conditions were applied to the model considering the actual physical setup of the gradient coil set in the MRI system i.e. the bottom face of the gradient coil set was constrained to have no permissible displacement or rotation in any direction.

Identification of the natural frequencies of gradient coil set is important to understand the vibration properties. The modal analysis is performed to evaluate the eigenvalues which are modal or natural frequencies and corresponding eigenvectors representing the mode shapes of the model under study. Considering the complexity of the model originating from geometry, contacts, layer interactions and boundary condition, the FEA software would show significantly high number of modes. In FEA model, the contact nodes between the adjacent layers were matched and to draw the meaningful results, the analysis frequency was limited to 5000 Hz. However, in real world system, not all natural frequencies would be excited as the excitation of natural frequencies purely depend on the nature and number of forcing functions.

To understand the realistic vibration behaviour of the gradient coil set, the harmonic analysis was performed. During image acquisition process, interaction of the main static magnetic field of the system and dynamic magnetic field produced by gradient coil leads to generation of Lorentz forces on the surface of gradient coil. These Lorentz forces and moments corresponding to 40 mT/m target gradient field strength in presence of 89mT static magnetic field were applied to the primary and shield gradient coils of FEA model as shown in Tab. 1. Please note that note that suffix 'p' represents primary gradient coil, and suffix 's' represents shield gradient coil.

Number	Gradient coil	Moment vector [Nm]	Force vector [N]
1	X_p	[0, 0, -6.8390]	[-0.1032, 2.4462E-032, 0]
2	Y_p	[0, 0, -8.5202]	[-0.1193, 3.6780E-33, 0]
3	Z_p	[0, 0, 0]	[-2.1939E-16, 1.5463E-15, 0]
4	X_s	[0, 0, 5.2115]	[0.0961, -3.6925E-33, 0]
5	Y_s	[0, 0, 6.3095]	[0.065, 1.6160E-32, 0]
6	\mathbf{Z}_{s}	[0, 0, 0]	[1.7482E-16, 2.5655E-16, 0]

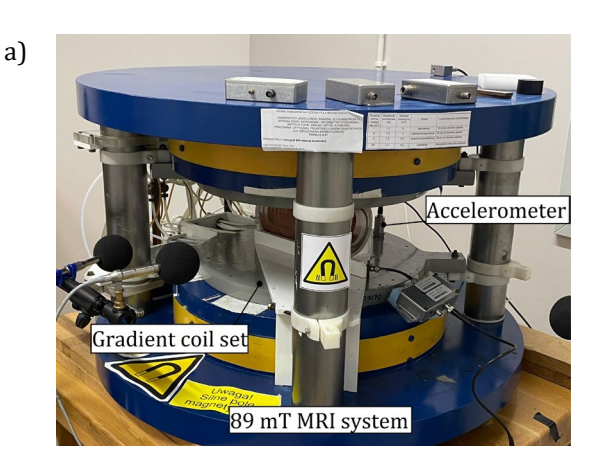
Table 1. The force and moment applied to the primary and shield gradient coils.

The harmonic analysis of the FE model with the frequency sweep from 1 to 5000 Hz was conducted to obtain the frequency response function (FRF) plot of the gradient coil set. To investigate the vibration characteristics in more detail, the FRFs were evaluated when all pairs of X, Y and Z coils were excited simultaneously and individually.

2.2. Experimental data collection

The vibration signals from the lower gradient coil set were recorded using piezoelectric type digital accelerometer (model: Digiducer 333D01 USB accelerometer). The accelerometer was connected to the computer placed in adjacent control room and the signals were stored for further analysis. The sampling frequency of the system was set to 12000 Hz to study the characteristics in frequencies 0-6000 Hz. The doped water container was placed inside the MRI scanning zone as a test specimen. The oscilloscope was used to identify association of gradient coil with type of gradient when operated for different orientations. The photograph of the experimental setup is shown in Fig. 2. The experimental measurements were undertaken for commonly used Spin Echo (SE) scanning sequence. For better understanding of the dynamics of the gradient coil set the slice selection gradient, phase encoding gradient and readout gradient were activated individually in transverse, coronal, and sagittal scanning orientations. The configuration of the MRI system for scanning sequence is shown in the Tab. 2, which remained constant during entire measurements.

The data collected from the accelerometer was processed and analysed using MATLAB® 2024a to investigate the gradient and orientation specific vibration behaviour of the coils. The time domain analysis was performed to investigate peak acceleration, Root-Mean-Squared (RMS) value and statistical measures of the signal which identifies the difference in amplitude or signal distribution for different gradient across different orientations.



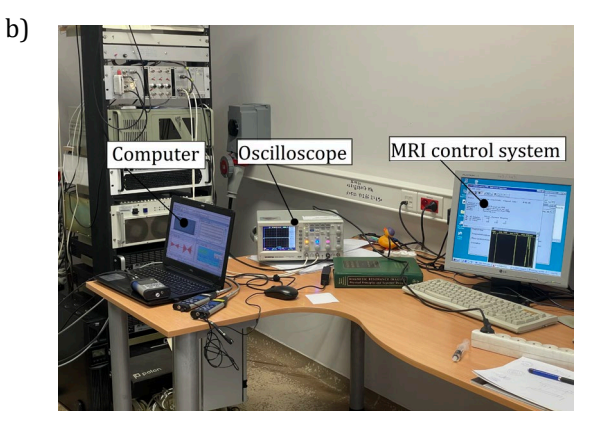


Figure 2. Measurement setup: a) MRI device b) control room setup.

Table 2. Configuration of the MRI system for experiments in Spin Echo Scanning sequence.

Parameter	Value	Units
Magnetic field strength B ₀	89	mT
Field of view (FOV)	200	mm
Number of slices	1	-
Slice thickness	200	mm
Repitition Time (TR)	1000	ms
Echo Time (TE)	100	ms

To study the characteristics of the signal in deep, the signals were transformed into frequency domain. The signals were filtered using the bandpass filter, to importantly focus on the frequency range of 100-5000 Hz. The Fast Fourier Transform (FFT) analysis of the signal was performed to plot the frequency spectrum and power spectral density (PSD) to evaluate the distribution of power over the frequency. The expression for evaluation of the PSD is shown in the Eq. 1:

$$S_{xx}(f) = \frac{1}{(N \cdot f_s)} |X(f)|^2, \tag{1}$$

where $S_{xx}(f)$ is the PSD of vibration signal, N is number of samples in time domain signal, f_s is the sampling frequency and X(f) is the Fourier transforms of discrete vibration signal. To compare the gradient coil vibration PSDs the coherence analysis was performed.

3. Results

3.1. FEA results

The modal analysis of FE model of the gradient coil set was performed in the frequency range of 1 to 5000 Hz. The application of boundary condition eliminated the rigid modes of the structure, as a result the structure could not execute translation or rotation without undergoing deformation. The gradient coil set showed more than 2500 modal frequencies within the frequency range analysed. Many symmetric modes showing similar vibration in different direction were identified occurring at slightly different frequencies. To interpret the physical significance of the resonant frequencies from the modal analysis it is important to correlate them with the results from harmonic analysis.

The harmonic analysis was performed for cases when all gradient coils were excited simultaneously and individually. The forcing function was swept for the frequency range of 1 to 5000 Hz to include all the possible frequencies during operation of MRI system. Since the top surface of lower gradient coil set is in contact with the scanning zone platform, the frequency response was evaluated on the topmost plane of FEA model. The results from the harmonic analysis were exported to MATLAB® for further processing. The amplitude of acceleration from the results were normalized for better understanding. The frequency response plots are plotted for orthogonal directions (X, Y and Z direction). Figure 3 depicts the results from frequency response when all pairs of X, Y and Z coils were excited individually and simultaneously. The frequency responses for individual excitation of pairs of X, Y and Z coils are shown in Figs. 3 a), b) and c), respectively and Fig. 3 d) depicts the frequency response for simultaneous excitation of all coils.

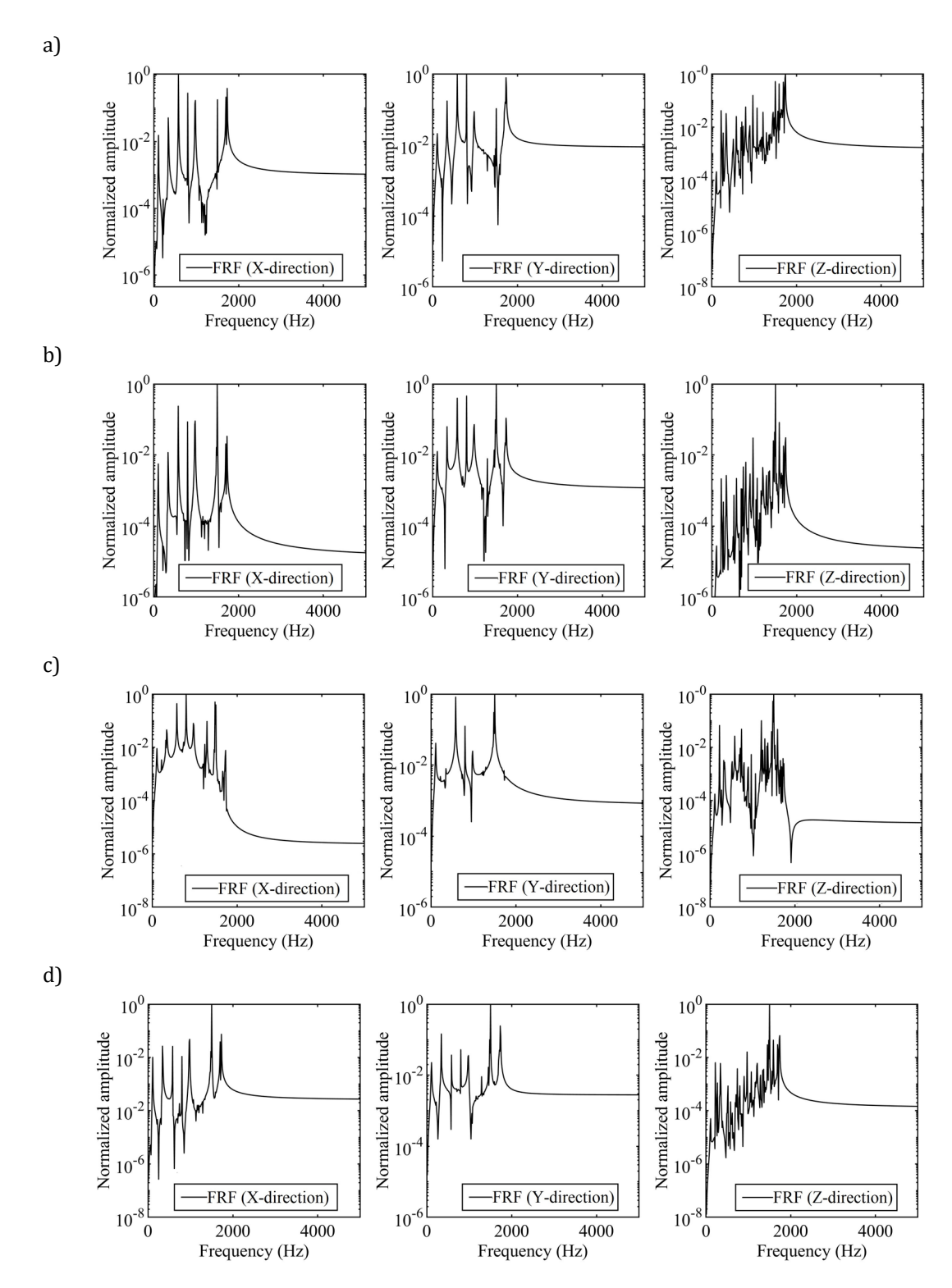


Figure 3. Orthogonal components of frequency response function (FRF) in vibration of top plane of gradient coil when excitation of (a) only X coils, (b) only Y coils, (c) only Z coils and (d) all coils together.

3.2. Results from experimental analysis

The acceleration signal from the lower gradient coil set was collected operating each individual gradient coil type across different orientations for Spin Echo scanning sequence. The sampling frequency was set to 12000 Hz as NEMA MS-4 2023 standard suggests the typical response of MRI system is observed below 5000 Hz [31]. The recorded time domain waveforms are shown in the Fig. 4. The amplitude of vibration for

slice gradient in all orientation was lower while it was highest for readout gradient in transverse and coronal orientation.

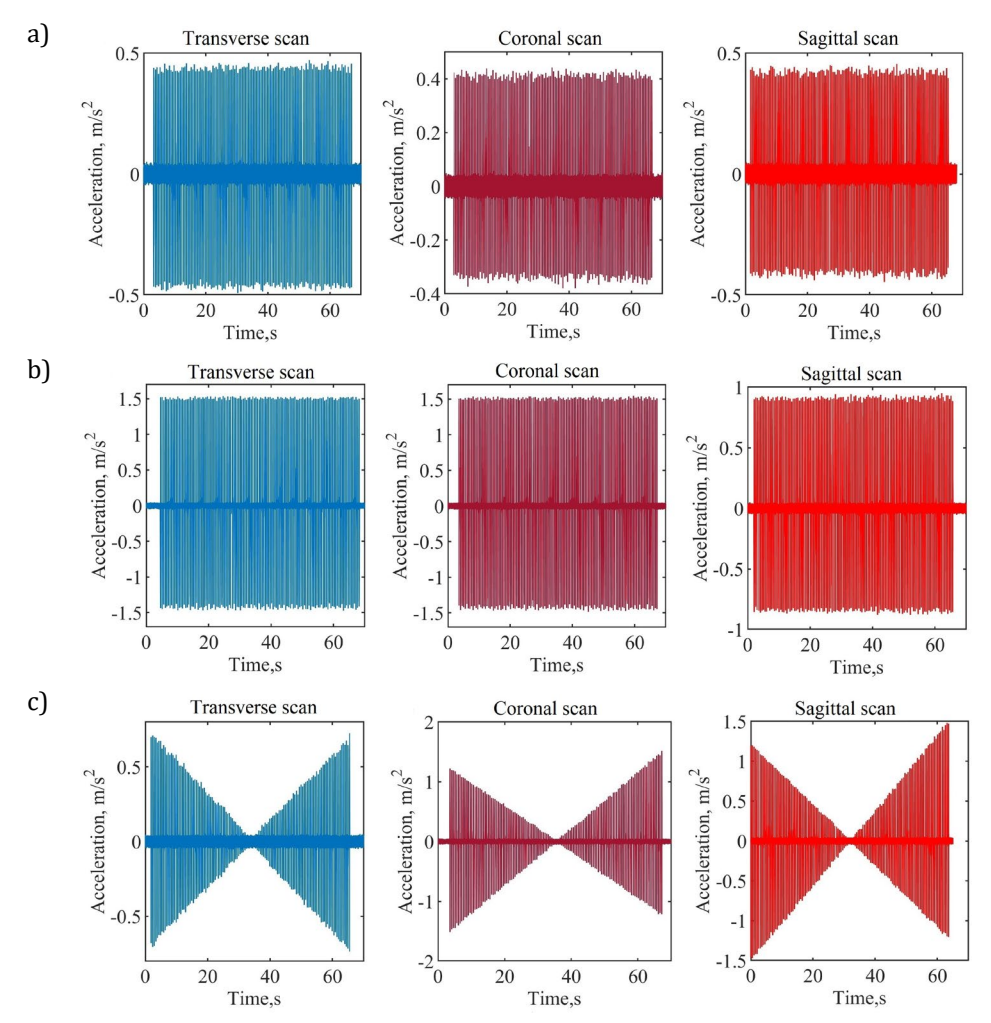


Figure 4. Time domain signal of the vibration signals recorded for different scan orientations with activation of individual a) slice, b) frequency readout, and c) phase encoding gradient types.

The time domain analysis of the recorded acceleration signals was performed to determine the peak and RMS acceleration and statistical characteristics. The silent parts in beginning and end were trimmed to increase correctness of the results. The results from time-domain analysis of the signals are presented in the Tab. 3.

Table 3. Results from the Time domain analysis of recorded acceleration signals for gradients in transverse (T), coronal (C) and sagittal (S) orientations.

Cuadianthuna	Acceleration (m/s ²)			Variance	Classenaga	Vuutosia
Gradient type	Peak	RMS	Mean	- Variance	Skewness	Kurtosis
Slice (T)	0.49	4.04E-02	1.00E-06	1.63E-03	-1.56E-01	45.70
Readout (T)	1.54	1.17E-01	4.00E-06	1.37E-02	5.81E-01	69.10
Phase encoding (T)	0.73	3.33E-02	-6.00E-06	1.11E-03	-5.40E-03	121.00
Slice (C)	0.44	2.86E-02	7.00E-06	8.20E-04	1.99E-01	44.40
Readout (C)	1.55	1.17E-01	-3.00E-06	1.37E-02	5.79E-01	68.90
Phase encoding (C)	1.52	4.94E-02	2.00E-06	2.44E-03	-3.27E-02	191.00
Slice (S)	0.46	3.13E-02	5.00E-06	9.82E-04	6.50E-01	52.70
Readout (S)	0.95	8.37E-02	-3.00E-06	7.00E-03	-1.97E-02	44.30
Phase encoding (S)	1.48	4.93E-02	3.00E-06	2.43E-03	-7.68E-02	191.00

The single sided FFT magnitude spectrum shown in Fig. 5 were plotted for each signal. To understand the relation between the applied gradient type in different orientations, PSD spectra was evaluated and compared as shown in the Fig. 6. To understand similarity between the vibration characteristics of gradient types in different orientations, the coherence analysis was performed. The coherence analysis is presented in the Fig. 7.

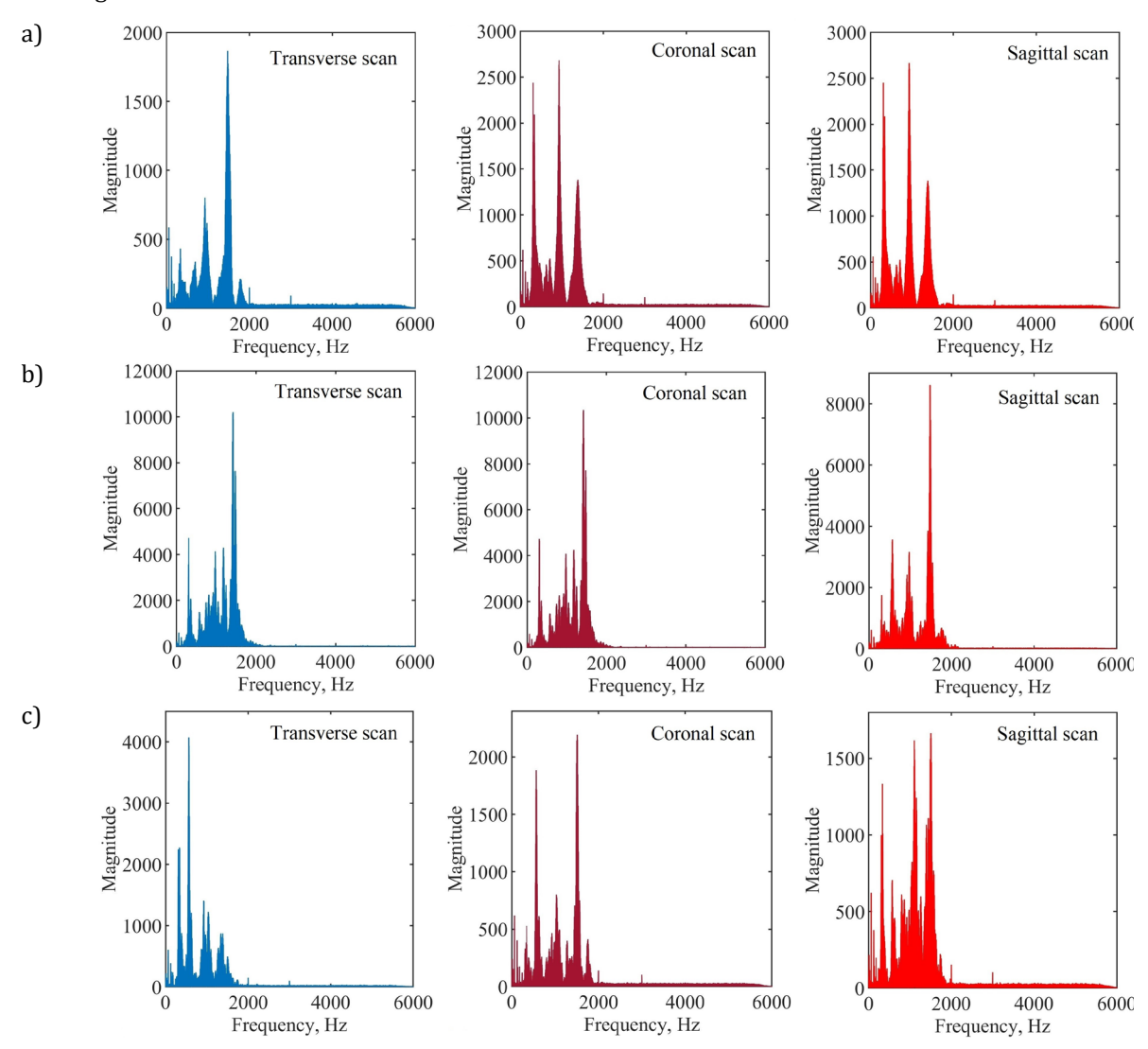


Figure 5. Single sided FFT spectrum of vibration measured for different gradient types in different scanning orientations to individually generate a) slice, b) frequency readout, c) phase encoding gradient.

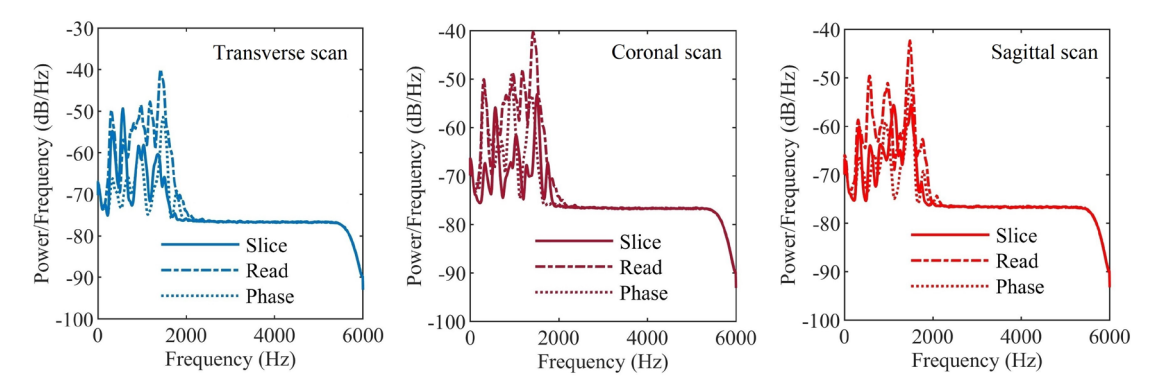


Figure 6. PSD of vibration signals for slice, readout and phase encoding gradient types in transverse, coronal and sagittal orientations.

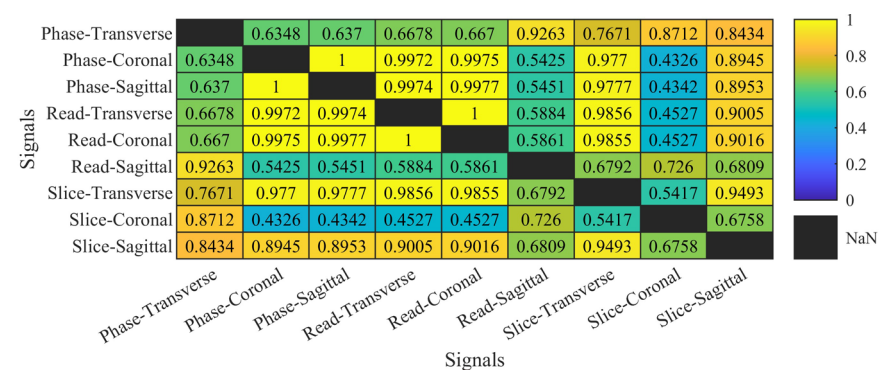


Figure 7. Coherence of gradient coil set vibration characteristics for different gradient types in different orientations.

3.3. Comprehensive comparison of FEA and experimental results

The important frequencies obtained from the experimental measurements and corresponding resonant frequency obtained from harmonic analysis (FEA) were identified. The mode shapes corresponding to the dominant peaks are presented in Fig. 8, while the comparison of FEA and experimental resonant frequencies is presented in the Fig. 9. The resonant frequencies below 300 Hz and greater than 1768 Hz were not predicted by the harmonic analysis of FEA model.

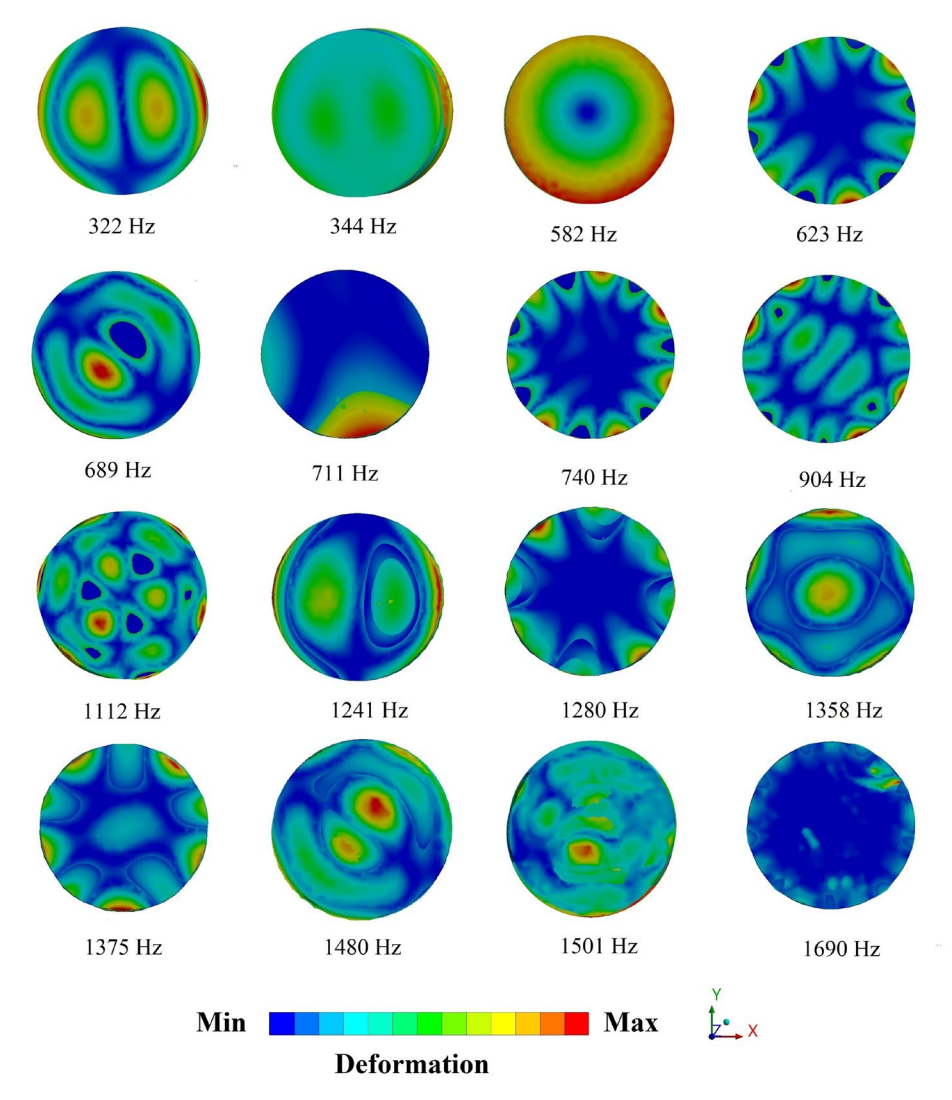


Figure 8. Mode shapes corresponding to resonant frequencies with dominant peaks.

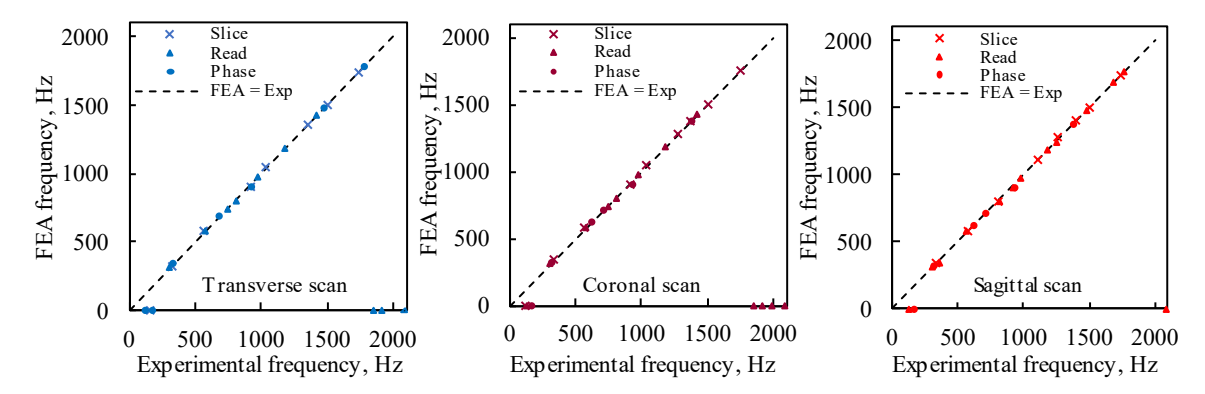


Figure 9. Comparison of experimental and FEA resonant frequencies for the slice, frequency readout and phase encoding gradient types in the transverse, coronal and sagittal scanning orientations.

4. Discussion

The detailed analysis of the vibration characteristics generated for slice, phase encoding and readout gradients in transverse, coronal and sagittal orientation offers deep insights about the dynamics of the system. The findings are important in determining vibration and noise reduction strategy. The scanned images from low field open configuration MRI system generally have less quality and resolution as compared to the closed configuration MRI system, hence vibrations reaching to the scanning area can degrade the scan quality and may generate false results [9,10]. Thus, it becomes essential to tackle the vibration issue to improve the performance of MRI scanner.

4.1. Finite element analysis

The finite element analysis of the vibration characteristics of lower gradient coil set is important as it is directly connected to the scanning zone with high possibility for transmission of vibrations. The modal analysis results revealed expected behaviour of system with significantly high number of natural frequencies in the frequency range of interest. Often, excitation of the structure at the natural frequencies lead to high magnitude of vibration and may cause problematic scenario. Hence characteristics of the system incorporating the forcing function reveals better understanding of the system dynamics. The harmonic analysis revealed distinct vibration characteristics for all cases of excitation. The FEA model results indicate that the application of forces and moments dictates the nature of vibration energy propagation through the layers and the occurrence of resonant frequencies. Frequency response plots presented in Fig. 3, show influence of excitation of different coils on the acceleration of top plane in x, y and z direction. The peak at the frequency 1500 Hz is consistent in all the FRFs. FRF plots for x and y direction clearly shows several peaks as usually observed in typical FRF. FRF in Z direction shows cluster of many resonant peaks, which can be interpreted to be originated from interaction of constituent layers in the model. Force and moment excitation in the coils induce shear, compression and tension in the layers of the model. This coupled behaviour of the layers can alter the resultant acceleration on the top layer. Simultaneous application of multiple forces and moments can amplify or diminish the cumulative vibration characteristics in the FEA model. Overall, the frequency response for all the cases shown no resonant frequencies in the range 2000 Hz to 5000 Hz.

4.2. Experimental analysis

4.2.1. Time domain analysis of operational vibration signal

The acceleration signal recorded for the three different gradient types revealed distinguishable patterns. The slice gradient in all scanning orientations, shown lower acceleration amplitude as compared to readout and phase encoding gradient. As shown in Tab. 2, slice gradient type presented maximum acceleration of 0.49 m/s² for scan in transverse orientation. In transverse and coronal scanning orientation, readout gradient shown almost similar vibration characteristics, while in coronal and sagittal orientations, the phase encoding gradient shown same vibration characteristics. The phase encoding gradient revealed special vibration pattern in which acceleration amplitude with each pulse gradually varies from maximum to zero and again to maximum. Skewness is statistical measure which highlights asymmetry of the probability distribution of the signal resulting in distinguishing the signal characteristics. The values of

skewness are between +1 and -1 and hence it can be said that these vibration signals are moderately skewed signifying the transient high energy events. The kurtosis values representing the peakedness in the signal are significantly high for all the signals. The maximum kurtosis is associated with the signals recorded for phase encoding gradient in all orientations. The time domain analysis reported the expected results adhering to the working principle of gradient coils.

4.2.2. Frequency domain analysis of vibration signals

To understand the vibration signal in more detail, they were transformed into frequency domain by using the FFT technique. The single sided magnitude spectrum referring to the Nyquist frequency were plotted for individual signals which shows the raw value of FFT amplitude corresponding to the frequency. To interpret the physical aspect of the signals it is important to study the PSD spectra. As shown in Fig. 6, PSD spectra of the gradient types in different orientations indicate multiple dominant peaks highlighting distribution of power in wide frequency range from 1-2000 Hz. The coherence analysis revealed that vibration signals for phase encoding gradient are identical in coronal and sagittal orientations, while it is having significantly different PSD spectra in transverse orientation. Similarly, readout gradient has identical PSD spectra in Transverse and Coronal orientation but different PSD spectra in Sagittal orientation. The slice gradient show similarity in PSD spectra only in Transverse and sagittal orientation. Vibration signal for slice gradient in coronal orientation and readout gradient in sagittal orientation show very low similarity towards others, except phase encoding gradient in transverse direction.

4.3. Comprehensive discussion of FEA and experimental study

In regular diagnostic procedure, scanning sequence involves combination of slice, phase encoding and readout gradients and hence it becomes important to understand the dynamic behaviour of the system. In the mode shapes of the gradient coil set presented in Fig. 8, it is important to note that the vibration patterns are complex and are result of layered structure of the system. The comparison of the key frequencies from PSDs of measured acceleration signals with predicted resonant frequencies in FEA model in presented average deviation 1.15 % with maximum deviation of 4.97 %. The peaks for frequencies lower than 305 Hz and greater than 1768 Hz observed in PSDs of experimental acceleration signals were not predicted by FEA model. In FE model, the constraint is applied at a base plane where absolutely no motion is possible, i.e. it behaves with infinite stiffness. But, in experimental condition the gradient coil set is mounted on the shim plate, which has finite stiffness. This complexity of the applied boundary condition in the FEA model can be the reason for deviation and absence of some resonant frequencies. Also, the Lorentz forces generated in the gradient coil are highly scanning sequence specific hence all the resonant frequencies identified during measurements could not be obtained in the FEA model.

The results confirm that the vibrations of gradient coil during scanning sequences are amplified due to resonant frequencies and reach to the top surface. slice, phase encoding and readout gradients show distinct vibration characteristics in different orientations and the important frequencies are clearly identified formulating better understanding from perspective to develop the vibration mitigation strategy. The previous studies on the MRI scanners also showed the high vibration energy peaks to be associated with the similar frequencies [32-35]. Also, the dominant frequency bands identified in this study are comparable to the frequencies associated with loud noise in the high field MRI operated for different scanning sequence, which was evaluated in our recent study [36] as well as other literature [37, 38]. Indicating the importance of this study in development of passive vibration and noise reduction strategy.

5. Conclusions

The study developed the FE model of the lower gradient coil set of the low field open configuration MRI scanner which accurately predict the vibration characteristics. The experimental validation of the FE model was performed by analysing the acceleration signals recorded on the top face of the lower gradient coil set. The signals were strategically recorded for different gradient types in different orientations to consider the dynamic behaviour of gradient coil set during scanning sequence. The results revealed that the harmonic analysis of FE model with application of resultant force and moment due to Lorentz force a predicted the resonant frequencies of system in very close agreement with average 1.15% deviation from the experimental resonant frequencies. All the important frequencies were identified in the frequency range below 2000 Hz. Also, the time and frequency domain analysis of the measured vibration signals sheds light on the dynamic characteristics revealing the gradient type and orientation specific behaviour. The results from the study are particularly valuable for designing and verification of vibration attenuation. The future work should explore the advanced materials and methods to improve the scan quality of the MRI scanners.

Acknowledgments

This work was supported and financed by Department of Mechanics and Vibroacoustics, Faculty of Mechanical Engineering and Robotics, AGH University in Kraków, Poland, from the finance source: 16.16.130.942.

Additional information

The authors declare: no competing financial interests and that all material taken from other sources (including their own published works) is clearly cited and that appropriate permits are obtained.

References

- 1. F. Bruno, F. Arrigoni, S. Mariani, A. Splendiani, E. Di Cesare, C. Masciocchi, A. Barile; Advanced magnetic resonance imaging (MRI) of soft tissue tumors: techniques and applications; Radiol. Med., 2019, 124, 243–252; DOI: 10.1007/s11547-019-01035-7
- 2. R. Reda, A. Zanza, A. Mazzoni, A. Cicconetti, L. Testarelli, D. Di Nardo; An Update of the Possible Applications of Magnetic Resonance Imaging (MRI) in Dentistry: A Literature Review; J. Imaging, 2021, 7(5), 75; DOI: 10.3390/jimaging7050075
- 3. L. Landini, L.T. Mainardi, V. Positano, A.A. Young, M. Santarelli, L. Ying, W.E. Kyriakos, A.J. den Dekker, M. Styner, Y.O. Halchenko, A. Frangi; Advanced image processing in magnetic resonance imaging, CRC press, 2018, DOI: 10.1201/9781420028669
- 4. C.K. Mannaerts, A. Kajtazovic, O.A.P. Lodeizen, M. Gayet, M.R.W. Engelbrecht, G.J. Jager, H. Wijkstra, T.M. de Reijke, H.P. Beerlage; The added value of systematic biopsy in men with suspicion of prostate cancer undergoing multiparametric MRI-targeted biopsy; Urologic Oncology: Seminars and Original Investigations, 2019, 37(5), 298.e1-298.e9; DOI: 10.1016/j.urolonc.2019.01.005
- 5. M. Viallon, V. Cuvinciuc, B. Delattre, L. Merlini, I. Barnaure-Nachbar, S. Toso-Patel, M. Becker, K.-O. Lovblad, S. Haller; State-of-the-art MRI techniques in neuroradiology: principles, pitfalls, and clinical applications; Neuroradiology, 2015, 57, 441–467; DOI: 10.1007/s00234-015-1500-1
- M.S. Maron, B.J. Maron; Clinical Impact of Contemporary Cardiovascular Magnetic Resonance Imaging in Hypertrophic Cardiomyopathy; Circulation, 2015, 132(4), 292–298; DOI: 10.1161/CIRCULATIONAHA.114.014283
- 7. E. Behluli, H.M. Preuer, N. Schiefermeier-Mach, R. Hornung, M. Küchler, M. Prokopetz; Patient-centric comparative analysis of experiences in open upright and conventional closed MRI scanners; Radiography, 2024, 30(5), 1258–1264; DOI: 10.1016/j.radi.2024.06.021
- 8. T.C. Arnold, C.W. Freeman, B. Litt, J.M. Stein; Low-field MRI: Clinical promise and challenges; Journal of Magnetic Resonance Imaging, 2023, 57(1), 25–44; DOI: 10.1002/jmri.28408
- 9. D. Gallichan, J. Scholz, A. Bartsch, T.E. Behrens, M.D. Robson, K.L. Miller; Addressing a systematic vibration artifact in diffusion-weighted MRI; Hum. Brain Mapp., 2010, 31(2), 193–202; DOI: 10.1002/hbm.20856
- 10. E. Fuhrer, M. Jouda, C.O. Klein, M. Wilhelm, J.G. Korvink; Gradient-Induced Mechanical Vibration of Neural Interfaces During MRI; IEEE Trans. Biomed. Eng., 2020, 67(3), 915–923; DOI: 10.1109/TBME.2019.2923693.
- 11. I. Frollo, P. Andris, J. Pribil, V. Juras; Indirect Susceptibility Mapping of Thin-Layer Samples Using Nuclear Magnetic Resonance Imaging; IEEE Trans. Magn., 2007, 43(8), 3363–3367; DOI: 10.1109/TMAG.2007.900571
- 12. S.S. Hidalgo-Tobon; Theory of gradient coil design methods for magnetic resonance imaging; Concepts in Magnetic Resonance Part A, 2010, 36(4), 223–242; DOI: 10.1002/cmr.a.20163
- 13. N. Gudino, S. Littin; Advancements in Gradient System Performance for Clinical and Research MRI; Journal of Magnetic Resonance Imaging, 2023, 57(1), 57–70; DOI: 10.1002/jmri.28421
- 14. S.A. Winkler, A. Alejski, T. Wade, C.A. McKenzie, B.K. Rutt; On the accurate analysis of vibroacoustics in head insert gradient coils; Magn Reson Med, 2017, 78(4), 1635–1645; DOI: 10.1002/mrm.26543
- 15. R.A. Hedeen, W.A. Edelstein; Characterization and prediction of gradient acoustic noise in MR imagers; Magn. Reson. Med., 1997, 37(1), 7–10; DOI: 10.1002/mrm.1910370103
- 16. P. Mansfield, P.M. Glover, J. Beaumont; Sound generation in gradient coil structures for MRI; Magn. Reson. Med., 1998, 39(4), 539–550; DOI: 10.1002/mrm.1910390406
- 17. A. Moelker, P.A. Wielopolski, P.M.T. Pattynama; Relationship between magnetic field strength and magnetic-resonance-related acoustic noise levels; MAGMA Magnetic Resonance Materials in Physics, Biology and Medicine, 2003, 16, 52–55; DOI: 10.1007/s10334-003-0005-9

- 18. S. Arawade, J. Piechowicz; Acoustic characterization of the 1.5 Tesla MRI facility in Mobile Imaging Trailer; Vibrations in Physical Systems, 2024, 34(2), 2024219; DOI: 10.21008/j.0860-6897.2024.2.19
- 19. R. Olivier, F. Le Moigne-Le Dem, P. Tétreault, D. Lorrain, V. Staehle; Characterization of Noise Produced During Continuous and Sparse Sampling Functional Magnetic Resonance Imaging; Canadian Acoustics, 2023, 51(3), 82–83
- 20. A. Moelker, P.M.T. Pattynama; Acoustic noise concerns in functional magnetic resonance imaging; Hum. Brain. Mapp., 2003, 20(3), 123–141; DOI: 10.1002/hbm.10134
- 21. J. Hutter, A.N. Price, L. Cordero-Grande, S. Malik, G. Ferrazzi, A. Gaspar, E.J. Hughes, D. Christiaens, L. McCabe, T. Schneider, M.A. Rutherford, J. V. Hajnal; Quiet echo planar imaging for functional and diffusion MRI; Magn Reson Med, 2018, 79(3), 1447–1459; DOI: 10.1002/mrm.26810
- 22. I. Bryjová, J. Kubicek, H. Skutova; Comparison and Classification of Acoustic Levels of MRI Sequences, in: XIV Mediterranean Conference on Medical and Biological Engineering and Computing 2016: MEDICON 2016, March 31st-April 2nd 2016, Springer Cham, Paphos, Cyprus, 2016, 774–778; DOI: 10.1007/978-3-319-32703-7_151
- 23. Y. Hu, Q. Wang, X. Hu, X. Zhu, S. Crozier, Y. Wang, F. Liu; A simulation study on the design of gradient coils in MRI for the imaging area above the patient bed; Meas. Sci. Technol., 2017, 28(3), 035402; DOI: 10.1088/1361-6501/aa56cd
- 24. Y. Wang; Gradient coil design and acoustic noise control in magnetic resonance imaging systems, PhD Thesis, University of Queensland, Australia, 2017
- 25. C.C. Sánchez, M.R. Cabello, Á.Q. Olozábal, M.F. Pantoja; Design of TMS coils with reduced Lorentz forces: application to concurrent TMS-fMRI; J. Neural. Eng., 2020, 17(1), 016056; DOI: 10.1088/1741-2552/ab4ba2.
- 26. Y. Wang, P. Xu, J. Zeng, J. Zhang, Y. Zhu, S. Che, C. Yao, Y. Ge, C. Wang; Sequence optimization for MRI acoustic noise reduction; J. Phys. Conf. Ser., 2023, 2591, 012034; DOI: 10.1088/1742-6596/2591/1/012034
- 27. T.C. Wood, N.L. Damestani, A.J. Lawrence, E. Ljungberg, G.J. Barker, A.B. Solana, F. Wiesinger, S.C.R. Williams; Silent myelin-weighted magnetic resonance imaging; Wellcome Open Res., 2020, 5, 74; DOI: 10.12688/wellcomeopenres.15845.2
- 28. N. Boulant, S. Ma, E. Walker, A. Beckett, A.T. Vu, S. Gunamony, D.A. Feinberg; Acoustic noise reduction in the NexGen 7 T scanner; Magn. Reson. Med., 2024, 92(5), 2261–2270; DOI: 10.1002/mrm.30211
- 29. S. Alibek, M. Vogel, W. Sun, D. Winkler, C.A. Baker, M. Burke, H. Gloger; Acoustic noise reduction in MRI using Silent Scan: an initial experience; Diagnostic and Interventional Radiology, 2014, 20(4), 360–363; DOI: 10.5152/dir.2014.13458
- 30. C. Leatherday, T. Fraser; Quantitative Phantom-Based Image Quality Analysis of MRI Acoustic Noise Reduction Algorithm Effects [Preprint], 2022; DOI: 10.21203/rs.3.rs-2188838/v1
- 31. NEMA MS 4-2023; Acoustic Noise measurement Procedure for Diagnostic Magneti Resonance Imaging (MRI) Devices, 2024
- 32. G.Z. Yao, C.K. Mechefske, Brian.K. Rutt; Acoustic noise simulation and measurement of a gradient insert in a 4T MRI; Applied Acoustics, 2005, 66(8), 957–973; DOI: 10.1016/j.apacoust.2004.11.006
- 33. J. Přibil, A. Přibilová, I. Frollo; Mapping and Spectral Analysis of Acoustic Vibration in the Scanning Area of the Weak Field Magnetic Resonance Imager; J. Vib. Acoust., 2014, 136(5), 051005; DOI: 10.1115/1.4027791
- 34. J. Přibil, A. Přibilová, I. Frollo; Analysis of spectral properties of acoustic noise produced during magnetic resonance imaging; Applied Acoustics, 2012, 73(8), 687–697; DOI: 10.1016/j.apacoust.2012.01.007
- 35. J. Přibil, A. Přibilová, I. Frollo; Comparison of mechanical vibration and acoustic noise in the open-air MRI; Applied Acoustics, 2016, 105, 13–23; DOI: 10.1016/j.apacoust.2015.11.013
- 36. S. Arawade, J. Piechowicz; Spectral Analysis of MRI Sound Signal; International Journal of Electronics and Telecommunications, 2024, 70(4), 839–847; DOI: 10.24425/ijet.2024.152068
- 37. S.A. Counter, A. Olofsson, H.F. Grahn, E. Borg; MRI acoustic noise: Sound pressure and frequency analysis; Journal of Magnetic Resonance Imaging, 1997, 7(3), 606–611; DOI: 10.1002/jmri.1880070327
- 38. M.E. Ravicz, J.R. Melcher, N.Y.-S. Kiang; Acoustic noise during functional magnetic resonance imaging; J. Acoust. Soc. Am., 2000, 108(4), 1683–1696; DOI: 10.1121/1.1310190
- © **2025 by the Authors.** Licensee Poznan University of Technology (Poznan, Poland). This article is an open access article distributed under the terms and conditions of the Creative Commons Attribution (CC BY) license (http://creativecommons.org/licenses/by/4.0/).